Analysis of dynamic systems with local nonlinearities

Analysis of dynamic systems with local nonlinearities:
1. Reduction of linear components
2. Determination of periodic solutions

R.H.B. Fey

W.F.W. report 89.054

October 1989

Eindhoven University of Technology
Department of Mechanical Engineering
Division of Physical and Mechanical Engineering Fundamentals

TNO–IBBC, Center for Mechanical Constructions
Delft, The Netherlands

Summary.

In this report nonlinear dynamic systems consisting of linear elastic components and local physical nonlinearities are studied. Examples of such nonlinearities are discrete nonlinear springs, discrete nonlinear dampers, dry friction, backlash etc. In general the linear components have many degrees of freedom. In order to obtain models which can be analysed with reasonable computational effort, the linear components are reduced using the component mode synthesis technique which makes use of low frequency, free interface eigenmodes and residual flexibility modes. The frequency criterion, which is used with reduction of linear systems, cannot be used in the same way with nonlinear systems. It is possible however, to check if the solution calculated with a nonlinear system model, of which the linear components have been reduced, is reliable by looking at the frequencyspectra of external loads minus the internal loads caused by the local nonlinearities.
The reduction technique is combined with a numerical method with which the steady state behaviour of nonlinear dynamic systems can be investigated. An important feature of this method, which is based on time discretisation, is that it is possible to investigate how a change in a so–called design variable influences the periodic equilibrium.

Contents:

1. Introduction.

In engineering practice many mechanical systems consisting of large complex components with linear elastic behaviour and local physical nonlinearities can be found. Examples of these systems are a pipeline supported by stiffening springs and the exhaust of a road vehicle in which dry friction hinges are found.

Currently the standard procedure to calculate a dynamic response is to compose a finite element model of the system, after which a numerical time integration method is applied to solve the (non)linear differential equations. In obtaining accurate information about displacements, strains and stresses often many elements must be used, which implies a great number of degrees of freedom (dof) in the model. In such cases numerical integration will lead to excessive computing times, especially when the nature of the integration method requires the timestep to be adjusted to the highest (momentary) eigenfrequency in the model.

In the next paragraph a component mode synthesis (cms) method, which offers a solution for these problems if the system only consists of linear components, will be treated. With cms methods component equations are reduced and subsequently the reduced component models are synthesized to get the reduced system model. The use of this reduction technique in case local nonlinearities are present is evaluated in paragraph three. By looking at frequencyspectra it is possible to check if the nonlinear system has been reduced properly after an analysis with the reduced system has been carried out. In a numerical study time response calculations of a nonlinear system with different levels of reduction will be compared. Numerical integration is unsuitable for determining steady state behaviour, especially with lightly damped systems. In paragraph four a numerical method based on a finite difference technique will be treated for the determination of steady state behaviour of nonlinear dynamic systems. This method, developed by Crooijmans (1987), is combined here with reduction of linear components. By applying an arc continuation method it is possible to investigate how a change in a so–called design variable influences the periodic equilibrium. Numerical examples will be presented.

2. Cms: reduction of linear components.

As mentioned before cms methods have two important features: division of the system in a number of components and reduction of component equations.
Distinguishing components offers several advantages. Only two are mentioned here. If the system has identical components only one component has to be modelled and analysed. If a component model has to be modified, only one component has to be analysed again. Subsequently a new synthesis of reduced component models and a new analysis on the reduced system model has to be carried out. This procedure takes far less computing time compared with a new analysis on the original system model.
The Ritz method is used to reduce the component equations: the coördinate–space of every component is approximated by a linear combination of a limited number of modes. By coupling the reduced component models we get the reduced system model, which will require much less CPU time to analyze than the original system model. A solution computed with a reduced model will be less accurate than a solution computed with the original model. However, by making a sensible selection of component modes this decrease of accuracy can be highly limited. We must require that those eigenmodes and eigenfrequencies of the original system model which substantially contribute to the response will be approximated well by the reduced system model. The important frequency range is determined by the frequency spectra of the external loads. Considering this, it would be convenient if the same frequency criterion could be used at component level. As has appeared from preceding research (Langeveld, 1986) this is possible with the cms method which makes use of low frequency free interface eigenmodes and residual flexibility modes. Thus, if we keep the free interface eigenmodes with eigenfrequencies up to a certain cut–off frequency f_c in every reduced component model, the eigenmodes of the reduced system model with eigenfrequencies up to f_c will form an accurate approximation of the same eigenmodes and –frequencies of the original system model. Probably it is sensible to choose the component cut–off frequency a bit higher, say $1.2\ f_c$, than the target frequency f_c of the system. Moreover the reduced system model will produce exactly the same solution as the original system model under static loads, provided that these loads act on dof for which residual flexibility modes have been defined. Because of these pleasant properties an ASKA process control program has been developed for this cms method.

We will now present a brief mathematical formulation of the cms method. The discretized equations of motion of a component are given by:

$$\underline{M}_x \ddot{\underset{\sim}{x}} + \underline{B}_x \dot{\underset{\sim}{x}} + \underline{K}_x \underset{\sim}{x} = \underset{\sim}{f}_x \qquad (2.1)$$

Column $\underset{\sim}{x}$ (n*1) will be partitioned into internal dof $\underset{\sim}{x}_I$ (n_I*1), which are not loaded and boundary dof $\underset{\sim}{x}_B$ (n_B*1), which are loaded by interface loads $\underset{\sim}{f}_{xif}$ (caused by neighbouring linear components and/or local nonlinear elements) and/or external loads $\underset{\sim}{f}_{xex}$:

$$\underset{\sim}{x} = \begin{bmatrix} \underset{\sim}{x}_I \\ \underset{\sim}{x}_B \end{bmatrix} \qquad (2.2)$$

$$\underset{\sim}{f}_x = \begin{bmatrix} \underset{\sim}{0} \\ \underset{\sim}{f}_{xif} + \underset{\sim}{f}_{xex} \end{bmatrix} \qquad (2.3)$$

The component is assumed to be proportionally damped, so that the free interface eigenmodes can be calculated by solving:

$$(-\omega_i^2 \underline{M}_x + \underline{K}_x) \underset{\sim}{\varphi}_i = \underset{\sim}{0} \qquad (i = 1, ..., n) \qquad (2.4)$$

The eigenfrequencies ω_i are collected in diagonal matrix $\underline{\Omega}$ (n*n) and the eigenmodes $\underset{\sim}{\varphi}_i$ columnwise in matrix $\underline{\Phi}$ (n*n). The latter are normed on the mass matrix $\underline{M}_x$:

$$\underline{\Phi}^T \underline{M}_x \underline{\Phi} = \underline{I} \qquad (2.5)$$

$$\underline{\Phi}^T \underline{K}_x \underline{\Phi} = \underline{\Omega}^2 \qquad (2.6)$$

In ASKA version 8.6, which is equiped with a Lanczos algorithm, it is possible to calculate only those eigenmodes with eigenfrequencies lying in a range of interest, which is in our case $0 - f_c$ Hz. Those angular eigenfrequencies and eigenmodes, which are kept in the component model, are stored in diagonal matrix $\underline{\Omega}_{KK}$ (n_K*n_K) respectively matrix $\underline{\Phi}_K$ (n*n_K). The deleted higher angular frequencies are stored in diagonal matrix $\underline{\Omega}_{DD}$ and the corresponding

deleted eigenmodes in matrix $\underline{\Phi}_D$ (n^*n_D). It is well known that, due to discretisation of the component into finite elements, the higher the number of an eigenfrequency and corresponding eigenmode, the greater will be the error in them. Therefore it seems not sensible at all to keep eigenfrequencies and –modes with numbers higher than, say 0.4 n, in the model.
To get a reduced system model with unaffected static load behaviour so called residual flexibility (rf) modes are defined for each boundary dof of a component. The rf modes appear to be important for the accuracy of eigenfrequencies ($<f_c$) and –modes of the reduced system model and also for the accuracy of frequency response functions near anti–resonances. The calculation of the rf modes is preceded by the determination of flexibility modes. A flexibility mode is defined as the static displacement field caused by an unit load acting on one boundary dof, whereas all other dof are not loaded. For a statically determinate component the matrix with flexibility modes $\underline{G}_A$ (n^*n_B) is given by:

$$\underline{G}_A = \underline{K}_x^{-1} \begin{bmatrix} \underline{0} \\ \\ \underline{I}_{BB} \end{bmatrix} \tag{2.7}$$

In case the component is able to move as a rigid body $\underline{K}_x^{-1}$ doesn't exist and an alternative formulation must and can be used, see Craig (1985) and Fey (1987). Using (2.6) the flexibility modes can be written as linear combinations of the eigenmodes:

$$\underline{G}_A = \underline{\Phi}\ \underline{\Omega}^{-2}\ \underline{\Phi}^T \begin{bmatrix} \underline{0} \\ \\ \underline{I}_{BB} \end{bmatrix} = \underline{\Phi}\ \underline{\Omega}^{-2}\ \underline{\Phi}_B^T \tag{2.8}$$

The matrix with rf modes $\underline{G}_B$ (n^*n_B) can be derived by subtracting from $\underline{G}_A$ the contribution of the kept eigenmodes $\underline{\Phi}_K$:

$$\underline{G}_B = \underline{G}_A - \underline{\Phi}_K\ \underline{\Omega}_{KK}^{-2}\ \underline{\Phi}_{KB}^T = \underline{\Phi}_D\ \underline{\Omega}_{DD}^{-2}\ \underline{\Phi}_{DB}^T \tag{2.9}$$

Having calculated all component modes we now put together the Ritz reduction matrix $\underline{T}_1$ ($n^*(n_K + n_B)$) and perform the following transformation:

$$\underset{\sim}{x} = \underline{T}_1 \underset{\sim}{p}_1 \quad \text{or} \quad \begin{bmatrix} \underset{\sim}{x}_I \\ \underset{\sim}{x}_B \end{bmatrix} = \begin{bmatrix} \underline{\Phi}_{KI} & \underline{G}_{BI} \\ \underline{\Phi}_{KB} & \underline{G}_{BB} \end{bmatrix} \begin{bmatrix} \underset{\sim}{p}_K \\ \underset{\sim}{p}_B \end{bmatrix} \tag{2.10}$$

In general $n_K + n_B$ will be much less than n. Using the second equation of (2.10) we bring $\underset{\sim}{x}_B$ explicitly in the dof set to permit simple coupling of the reduced component equations:

$$\underset{\sim}{p}_1 = \underline{T}_2 \underset{\sim}{p} \quad \text{or} \quad \begin{bmatrix} \underset{\sim}{p}_K \\ \underset{\sim}{p}_B \end{bmatrix} = \begin{bmatrix} \underline{I} & \underline{0} \\ -\underline{G}_{BB}^{-1} \underline{\Phi}_{KB} & \underline{G}_{BB}^{-1} \end{bmatrix} \begin{bmatrix} \underset{\sim}{p}_K \\ \underset{\sim}{x}_B \end{bmatrix} \tag{2.11}$$

Combining (2.10) and (2.11) gives:

$$\underset{\sim}{x} = \underline{T} \underset{\sim}{p} \tag{2.12}$$

$$\underline{T} = \underline{T}_1 \underline{T}_2 \tag{2.13}$$

Substitution of (2.12) in (2.1), followed by premultiplication with the transposed of $\underline{T}$ results in the reduced component equations:

$$\underline{M}_p \ddot{\underset{\sim}{p}} + \underline{B}_p \dot{\underset{\sim}{p}} + \underline{K}_p \underset{\sim}{p} = \underset{\sim}{f}_p \tag{2.14}$$

where $\underline{M}_p = \underline{T}^T \underline{M}_x \underline{T}$, $\underline{B}_p = \underline{T}^T \underline{B}_x \underline{T}$, $\underline{K}_p = \underline{T}^T \underline{K}_x \underline{T}$ and $\underset{\sim}{f}_p = \underline{T}^T \underset{\sim}{f}_x$.

When all component equations have been reduced we can assemble the reduced system model by demanding compatibility of interface dof and equilibrium of interface loads. We define $\underset{\sim}{q}$ (n_q*1) as the column with independent dof of the reduced system model.

$\underset{\sim}{q}$ consists of modal dof $\underset{\sim}{p}_k^{(i)}$ (i = 1, ..., N) belonging to N linear components and $\underset{\sim}{x}_T$, containing all boundary dof of the system:

$$\underset{\sim}{q}^T = [\underset{\sim}{p}_K^{(1)^T}, \ ..., \ \underset{\sim}{p}_K^{(N)^T}, \quad \underset{\sim}{x}_T^T] \tag{2.15}$$

For each component (i) a backtransformation matrix can be formed which relates $\underset{\sim}{q}$ to the original component dof $\underset{\sim}{x}^{(i)}$. This matrix is the product of

matrix $\underline{T}^{(i)}$, see (2.13), and a Boolean matrix $\underline{S}^{(i)}$:

$$\underset{\sim}{x}^{(i)} = \underline{T}^{(i)}\ \underline{S}^{(i)}\ \underset{\sim}{q} \qquad (i = 1, \ldots, N) \tag{2.16}$$

The mass matrix of the reduced system model $\underline{M}_q$ $(n_q * n_q)$ is calculated by:

$$\underline{M}_q = \sum_{i=1}^{N} \underline{S}^{(i)^T}\ \underline{M}_p^{(i)}\ \underline{S}^{(i)} \tag{2.17}$$

Stiffness matrix $\underline{K}_q$ $(n_q * n_q)$ and damping matrix $\underline{B}_q$ $(n_q * n_q)$ are calculated by similar expressions. In the column with loads $\underset{\sim}{f}_q$ $(n_q * 1)$ all interface loads $\underset{\sim}{f}_{xif}^{(i)}$ have disappeared, so that only external loads remain:

$$\underset{\sim}{f}_q = \sum_{i=1}^{N} \underline{S}^{(i)^T}\ \underset{\sim}{f}_p^{(i)} = \sum_{i=1}^{M} \underline{S}^{(i)^T}\ \underset{\sim}{f}_{xex}^{(i)} = \tag{2.18}$$

$$[\underset{\sim}{0}^{(i)^T}, \ldots, \underset{\sim}{0}^{(N)^T}, \underset{\sim}{f}_{qT}^T]^T$$

The equations of motion of the reduced system model finally are given by:

$$\underline{M}_q\ \ddot{\underset{\sim}{q}} + \underline{B}_q\ \dot{\underset{\sim}{q}} + \underline{K}_q \underset{\sim}{q} = \underset{\sim}{f}_q \tag{2.19}$$

As stated before the (damped) eigenfrequencies of (2.19) below f_c Hz will be very accurate. The error in eigenfrequencies above f_c Hz however will increase very rapidly. If one is willing to sacrifice a static 'exact' model and high accuracy near anti–resonances in the range 0–f_c Hz these higher (artificial) eigenfrequencies can be deleted by reducing (2.19) one more time.
We present an example to show the benefits of the cms method:

Example 2.1: Consider the in plane vibrations of the pin ended double cross (fig. 2.1), also studied by Morris (1989). As frequency range of interest has been chosen: 0–100 Hz. We made two eigenfrequency analyses. In the first analysis the system was seen as one component composed of 400 beam elements (1187 dof). The analyses, in which 16 eigenfrequencies and –modes were calculated, costed 768 seconds CPU time. Some of the eigenmodes are

shown in fig. 2.2. In the second analysis the system was divided into 8 components of 50 elements each. One component was reduced using a cut–off frequency of 120 Hz, which meant that 4 free interface eigenmodes (among them one rigid body mode) were kept in the component model, next to three rf modes. This model was rotated seven times, after which the reduced system model (35 dof) was synthesized. All together the second analysis costed 130 seconds CPU time, which is about 6 times less compared with the first analysis. When the eigenfrequencies calculated with both analyses are compared (table 2.1), we find a maximum relative difference of 9E–4% below 100 Hz, which is a good result.

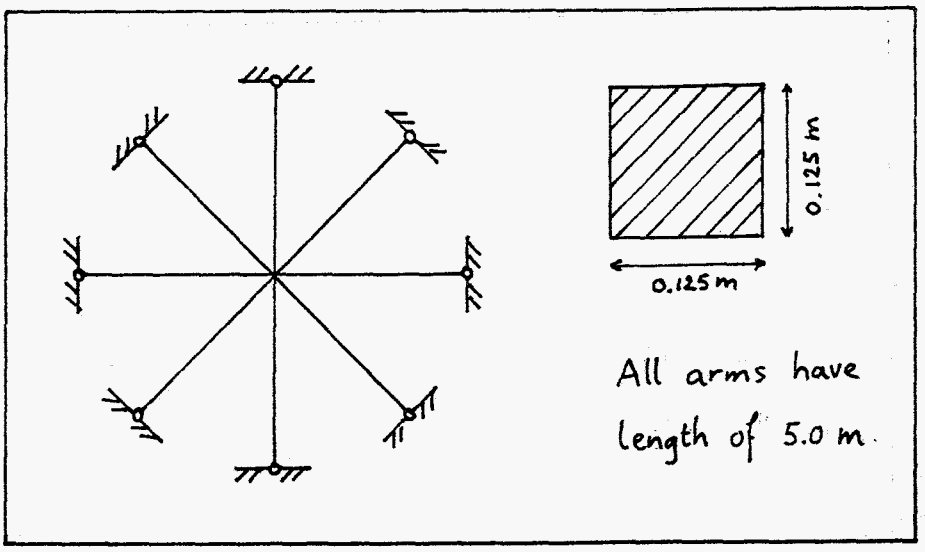

Fig. 2.1 Pin ended double cross (E = 2.0 E11 N/m^2, ρ = 8000 kg/m^3).

Mode (–)	Reference frequency Morris (Hz)	Analysis 1 (Hz)	Analysis 2 (Hz)
1	11.336	11.3363	11.3363
2–3	17.709	17.6808	17.6808
4–8	17.709	17.7094	17.7094
9	45.345	45.3450	45.3451
10–11	57.390	57.0746	57.0751
12–16	57.390	57.3898	57.3902

Table 2.1 Eigenfrequencies pin ended double cross.

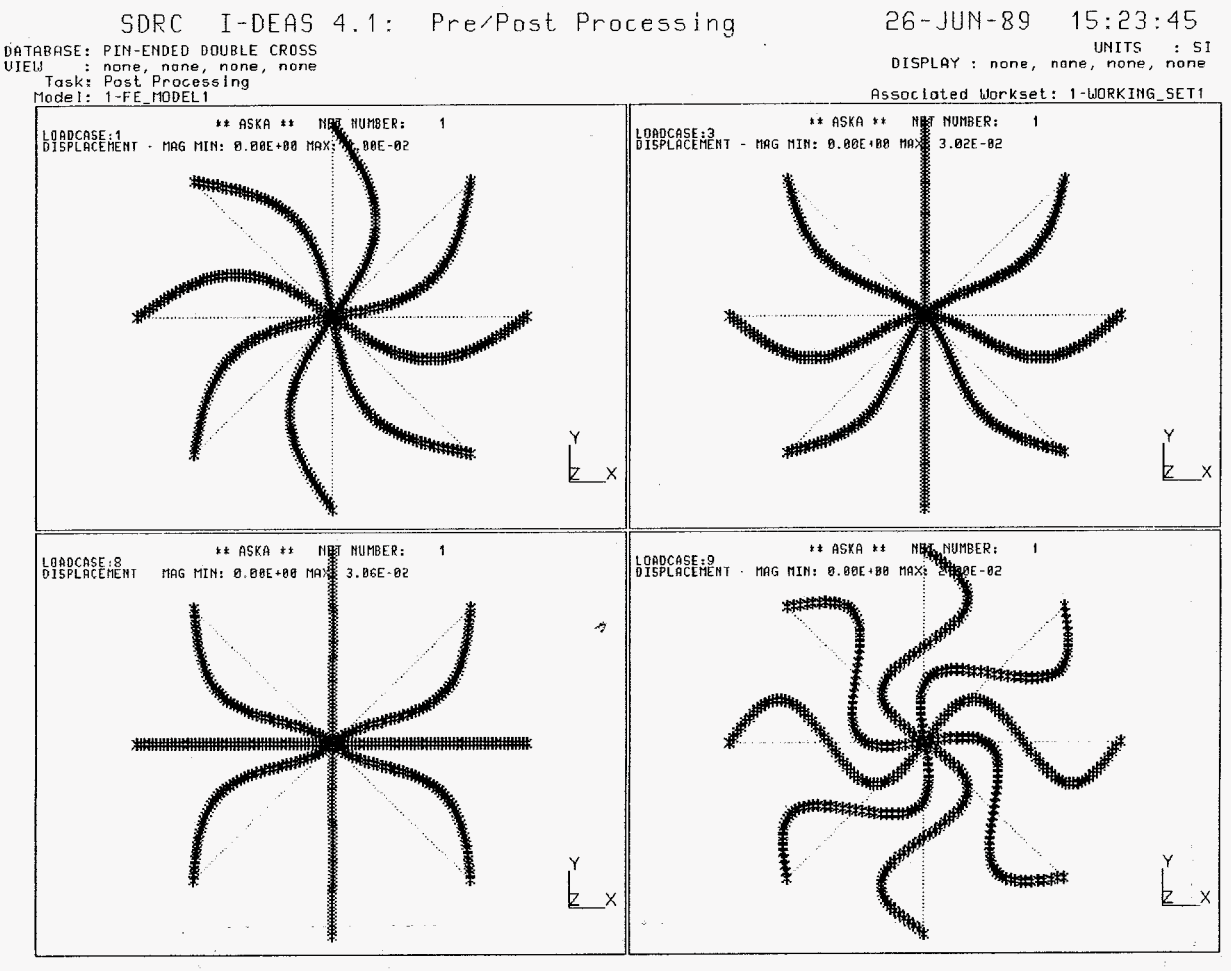

Fig. 2.2 Some eigenmodes of the pin ended double cross (loadcase i corresponds with eigenmode i).

3. Addition of local nonlinearities and numerical integration.

Local nonlinearities are added to (2.19) by means of a column with internal loads $\underset{\sim}{f}_{nl}$ (n_q*1). Local nonlinearities act on boundary dof $\underset{\sim}{x}_T$ and it is assumed here that no extra dof are introduced:

$$\underline{M}_q\ddot{\underset{\sim}{q}}(t) + \underline{B}_q\dot{\underset{\sim}{q}}(t) + \underline{K}_q\underset{\sim}{q}(t) + \underset{\sim}{f}_{nl}(\ddot{\underset{\sim}{x}}_T,\dot{\underset{\sim}{x}}_T,\underset{\sim}{x}_T,t) = \underset{\sim}{f}_q(t) \qquad (3.1)$$

$$\text{with } \underset{\sim}{f}_{nl}^T = [\underset{\sim}{0}^{(1)^T}, \ldots, \underset{\sim}{0}^{(N)^T}, \underset{\sim}{f}_{nlT}^T]$$

Of course (3.1) always can be integrated numerically, but the value of the solution must be judged critically. In fact the important eigenfrequencies and –modes of the coupled linear component now are determined by the frequency spectra of $\underset{\sim}{f}_q - \underset{\sim}{f}_{nl}$, which only can be calculated <u>after</u> integrating (3.1). But then again these spectra might considerably change if we would increase the number of kept modes in the component models. If addition of component modes has negligible influence on the frequency spectra of $\underset{\sim}{f}_q - \underset{\sim}{f}_{nl}$ <u>and</u> if all important frequencies of the spectra are present in the linear component models, we have succeeded in reducing the system model in a sensible way. We will illustrate this strategy with an example:

Example 3.1 (all quantities in SI units): Consider the 1D system shown in fig. 3.1. A continuous linear bar (mass density = 5, cross section = 0.1, modulus of elasticity = 15, length = 3) is clamped at its right end and coupled with a single degree of freedom system of the Duffing type at its left end. The homogeneous differential equation of the Duffing system is given by: $0.5\,\ddot{x} + 0.02\,\dot{x} + 0.5\,x + 0.04\,x^3 = 0$. The bar is modelled with 50 elements.

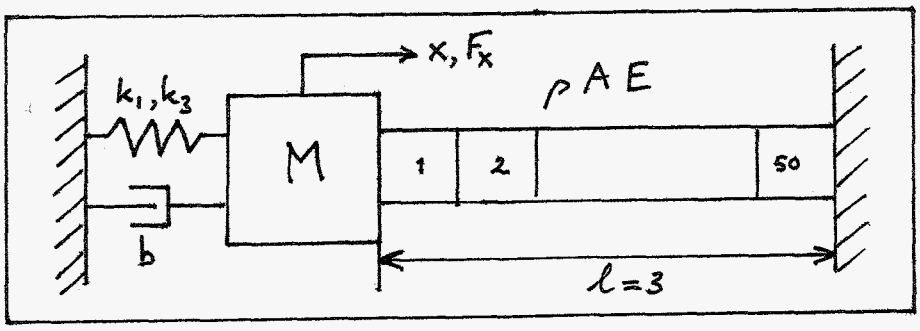

Fig. 3.1 Bar coupled with sdof Duffing system.

The first 16 eigenfrequencies of the undamped linear component (i.e. the bar plus the discrete mass and the linear part of the spring of the Duffing system) are presented in table 3.1.
Numerical integration was carried out with the variable order, variable step routine D02CBF of the NAG Fortran library (1988). In each analysis an accuracy of 6 decimal places was demanded.

i	f_i	i	f_i	i	f_i	i	f_i
1	0.1504	5	1.1793	9	2.3448	13	3.5541
2	0.3589	6	1.4667	10	2.6427	14	3.8647
3	0.6187	7	1.7569	11	2.9433	15	4.1791
4	0.8957	8	2.0496	12	3.2470	16	4.4976

Table 3.1 Eigenfrequencies (Hz) of undamped linear component.

At first, starting with zero initial conditions, the discrete mass was loaded by the periodic force $F_x = \sin(2\pi ft)$ where $f = 0.38$ Hz. We reduced the component by keeping 3 eigenmodes ($f_c = 0.7$ Hz) plus 1 rf mode in the model. Subsequently the internal load $F_{nl} = 0.02\,\dot{x} + 0.04\,x^3$ was added. The reduced system model (called 4C) was integrated over the time interval $0 - 1000$ s. The frequency spectra of x and load $F_x - F_{nl}$ are shown in fig. 3.2 respectively fig. 3.3. When we look at fig. 3.3 we find two frequency ranges (near 0.9 Hz and 1.14 Hz) above f_c which might significantly change the solution if eigenmodes 4 and 5 would be kept in the component model. This was checked with a second analysis (model 6C, $f_c = 1.2$ Hz $\simeq 3f$) which resulted in the frequency spectra shown in fig. 3.4 (x) and fig. 3.5 (load). Comparing fig. 3.2 with fig. 3.4 we notice that the peak at 1.02 Hz (artificial eigenfrequency of 4C) visible in fig. 3.2 has disappeared in fig. 3.4 and a new peak is found at $f_4 = 0.8957$ Hz. The (numerical values of the) frequency spectrum of the load did not change significantly so it is believed that we obtained a reasonable accurate solution with model 6C. We verified this by keeping 20 eigenmodes in the component model and integrating again. Now both the frequency spectra of x (fig. 3.6) and the load (fig. 3.7) did not change significantly. The time response resulting from this third analysis (model 21C) is shown in fig. 3.8. The greatest differences found in x(t) were 3.0 E–2 (4C – 21C) and 5.1 E–4 (6C – 21C). The costs for integration in

terms of CPU time were: 356 s (4C), 576 s (6C) and 5852 s (21C). Even if we count up the CPU times of 4C and 6C costs are diminished by a factor 6.3.

We made a second calculation with models 4C, 6C and 21C: again starting with zero initial conditions the discrete mass now was loaded with $F_x = \sin(2\pi\ 0.368\ t)$ during 400 s; subsequently the frequency was continuously increased to 0.38 Hz over an interval of 600 s and then kept constant during 1000 s. When we look at the time response calculated with model 21C (fig. 3.9) we see that the steady state which was reached now differs completely from the steady state reached in fig. 3.8. We will return to this phenomenon in example 4.1. The greatest differences found in x(t) during the last 1000 s were –0.24 (4C – 21C) and 3.0 E–3 (6C – 21C). The CPU times were: 1024 s (4C), 1522 s (6C) and 11983 s (21C). The frequency spectra of x and the load during the last 1000 s are shown in fig. 3.10 – 3.15. When comparing the frequency spectra of x and the load of the two analyses 6C and 21C again no significant differences are found. The peak in the load spectrum at 5f = 1.9 Hz does lie above f_c = 1.2 Hz (6C), but is not near an eigenfrequency of the component.

So again 6C provides an accurate and cheap solution. Because of the hight of the amplitude of the steady state F_{nl} now dominates F_x, whereas the opposite was the case in the first calculations. This can be concluded when we examine fig. 3.10 – 3.15 where higher harmonics (3f, 5f, 7f) of the excitation frequency f play a much more important role than in fig. 3.2 – 3.7. (at 5f and 7f, not visible in fig. 3.2 – 3.7, no peaks were found).

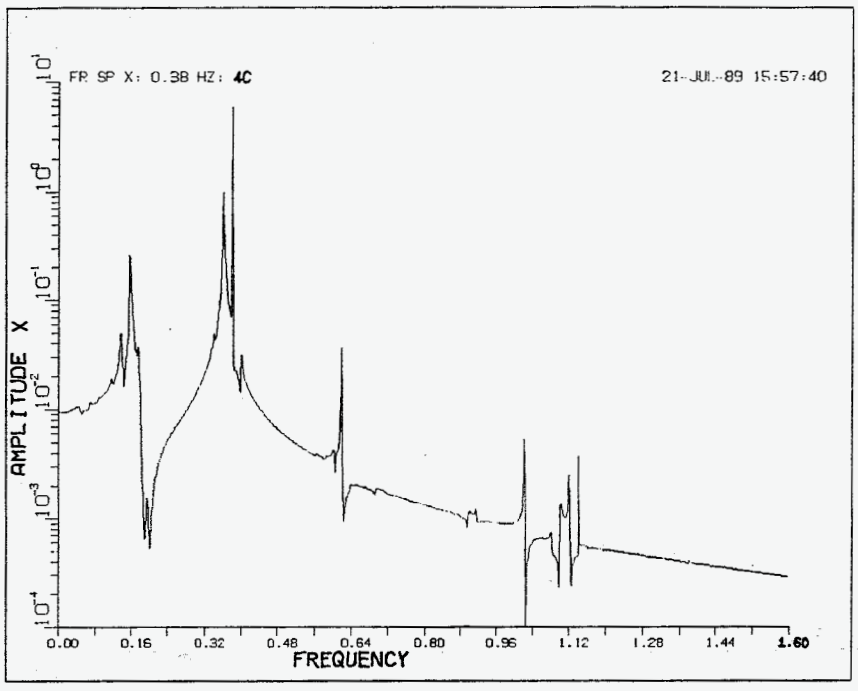

Fig. 3.2 *Frequency spectrum of x, low stable steady state, excitation* $F_x = \sin(2\pi\ 0.38\ t)$, *model 4C.*

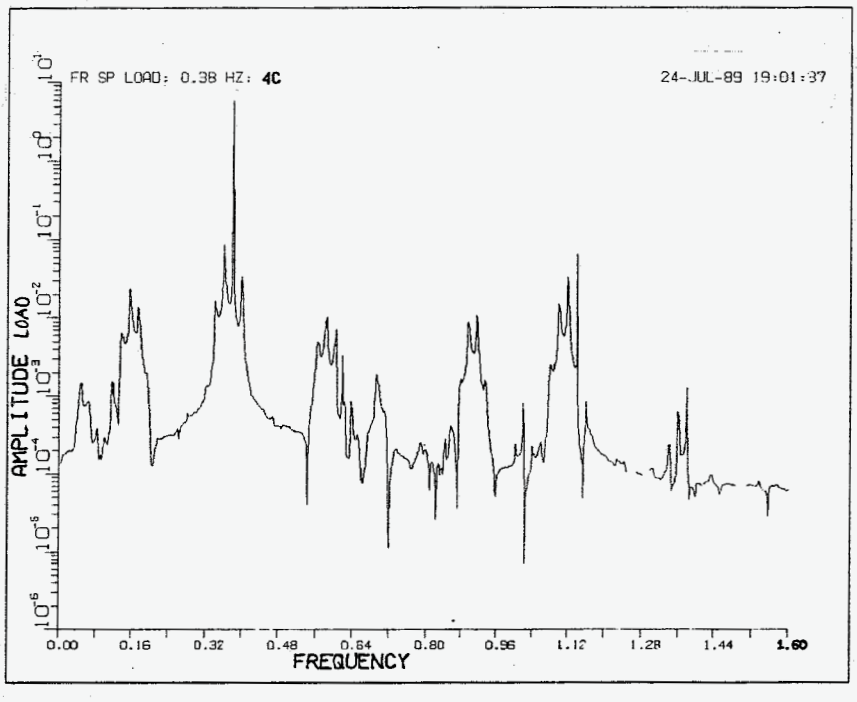

Fig. 3.3 *Frequency spectrum of* $F_x - F_{nl}$, *low stable steady state, excitation* $F_x = \sin(2\pi\ 0.38\ t)$, *model 4C.*

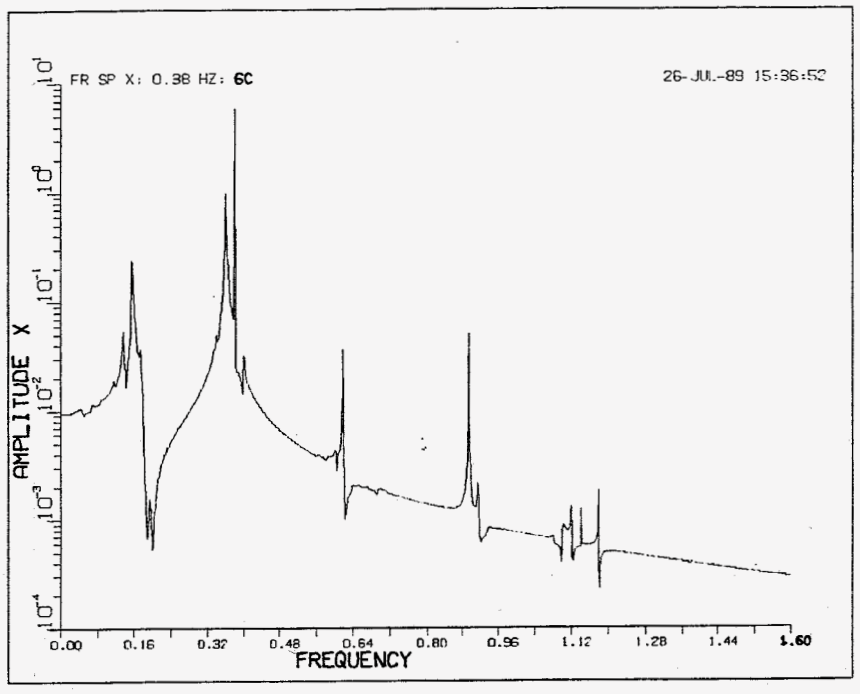

Fig. 3.4 *Frequency spectrum of x, low stable steady state, excitation* $F_x = \sin(2\pi\ 0.38\ t)$, *model 6C.*

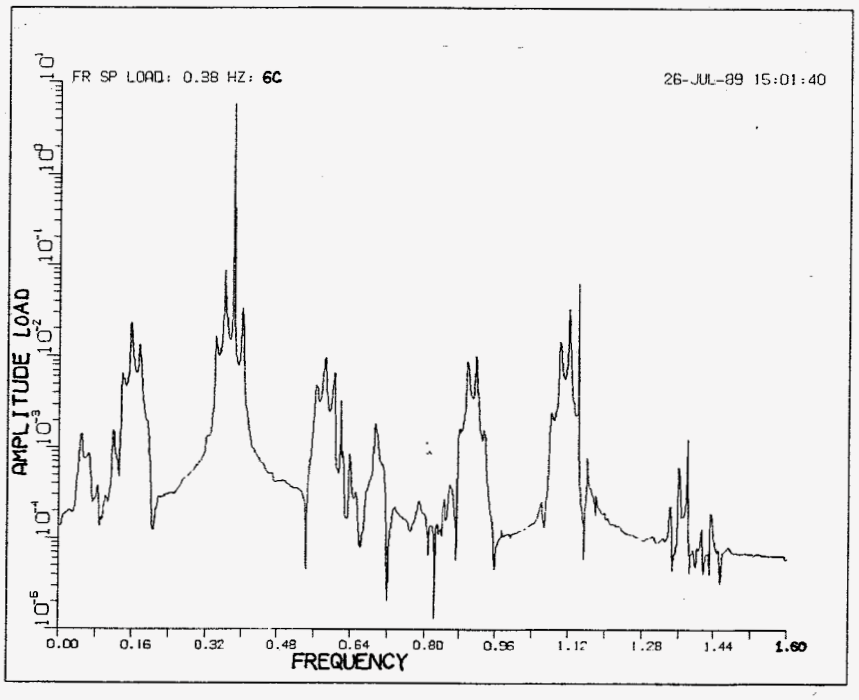

Fig. 3.5 *Frequency spectrum of* $F_x - F_{nl}$, *low stable steady state, excitation* $F_x = \sin(2\pi\ 0.38\ t)$, *model 6C.*

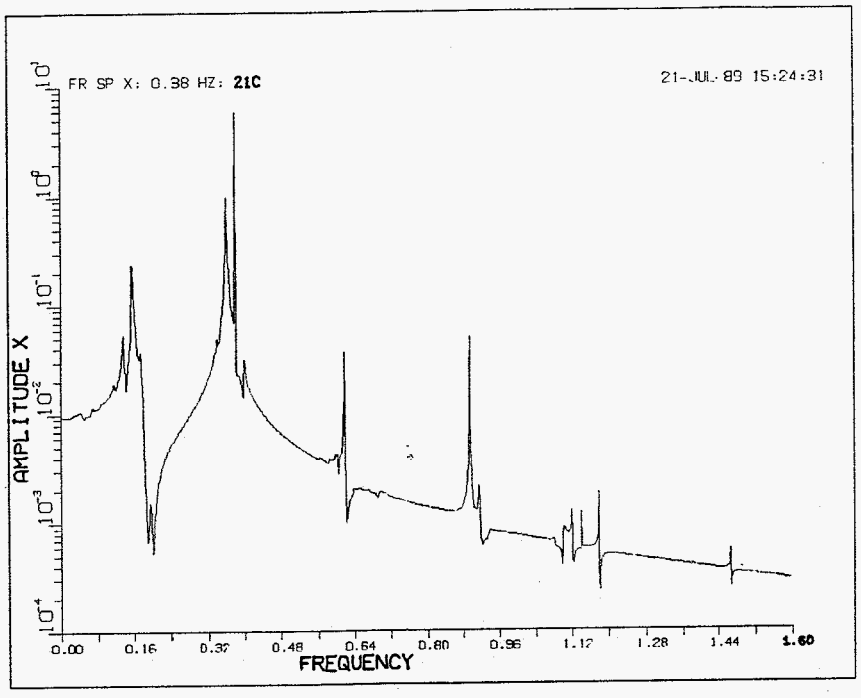

Fig. 3.6 *Frequency spectrum of x, low stable steady state, excitation* $F_x = \sin(2\pi\ 0.38\ t)$, *model 21C.*

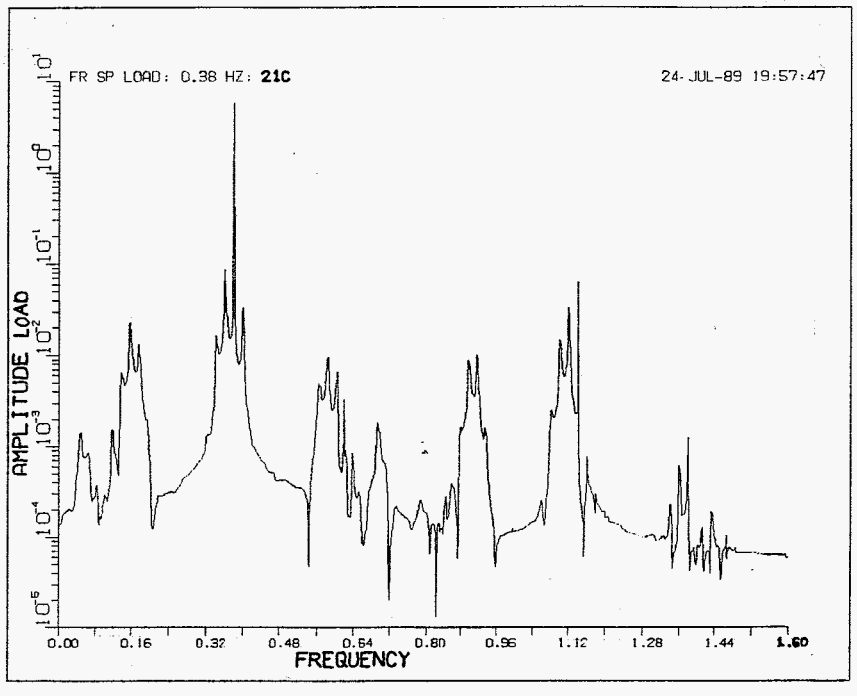

Fig. 3.7 *Frequency spectrum of* $F_x - F_{nl}$, *low stable steady state, excitation* $F_x = \sin(2\pi\ 0.38\ t)$, *model 21C.*

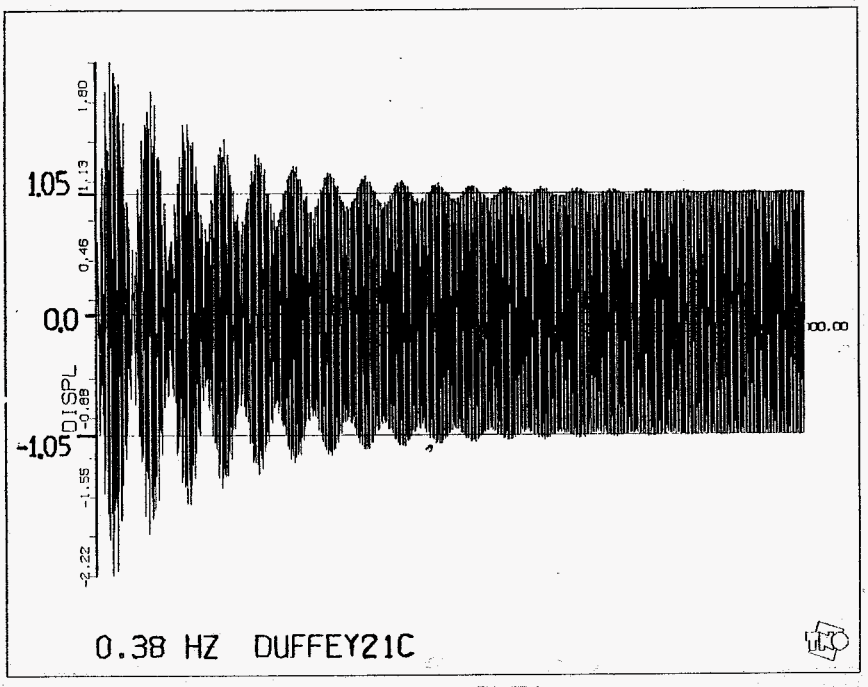

Fig. 3.8 *Time response x(t), low stable steady state, excitation F_x = sin(2π 0.38 t), zero initial conditions, model 21C.*

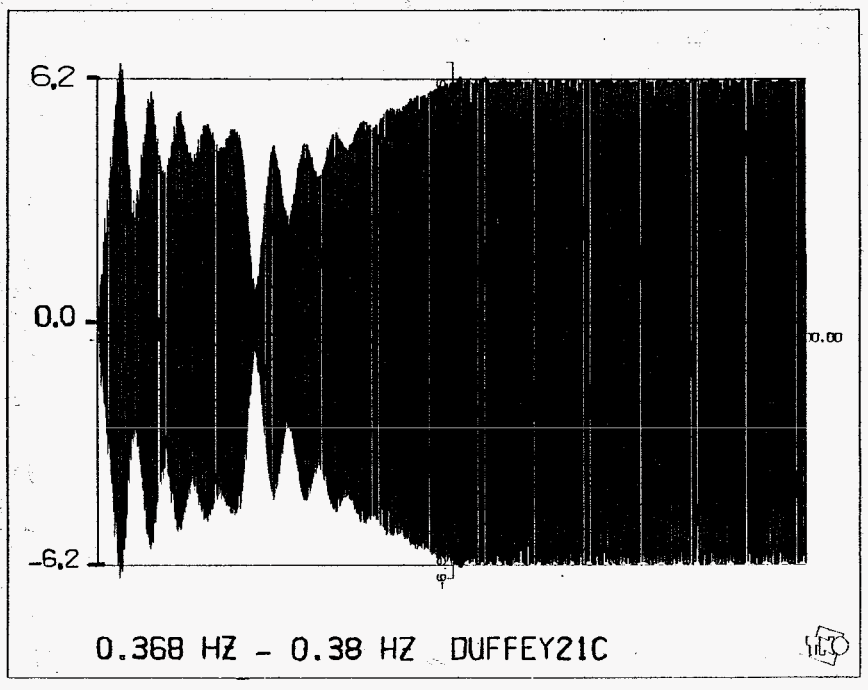

Fig. 3.9 *Time response x(t), high stable steady state, excitation F_x = sin(2π 0.38 t), frequency sweep f= 0.368 Hz -> 0.38 Hz, model 21C.*

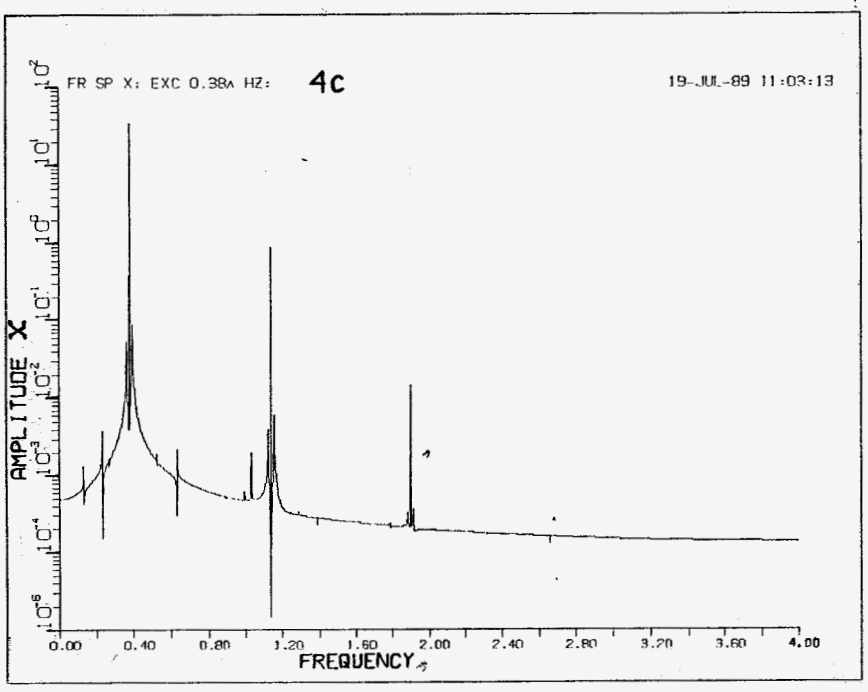

Fig. 3.10 *Frequency spectrum of x, high stable steady state, excitation* $F_x = \sin(2\pi\ 0.38\ t)$, *model 4C.*

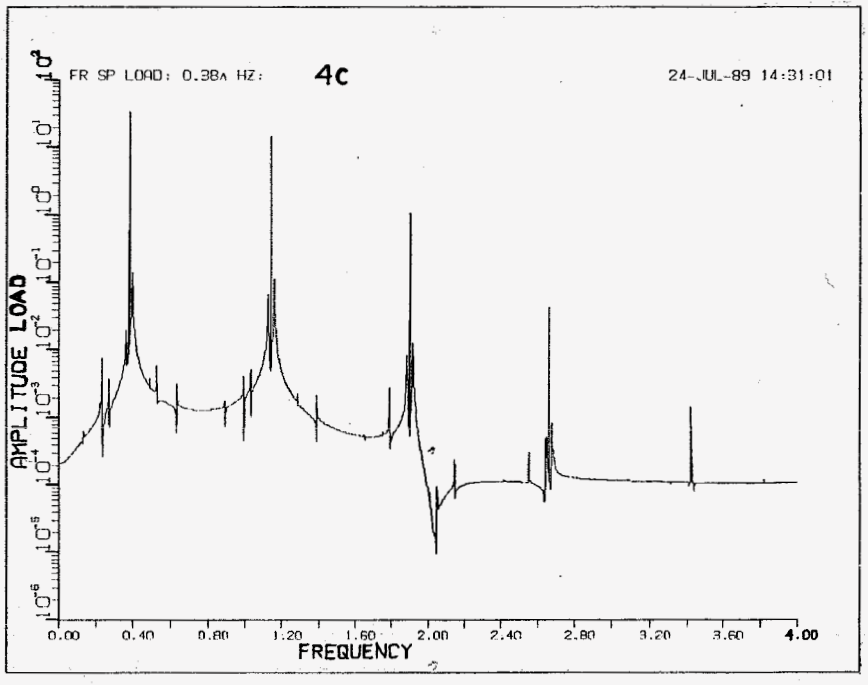

Fig. 3.11 *Frequency spectrum of* $F_x - F_{nl}$, *high stable steady state, excitation* $F_x = \sin(2\pi\ 0.38\ t)$, *model 4C.*

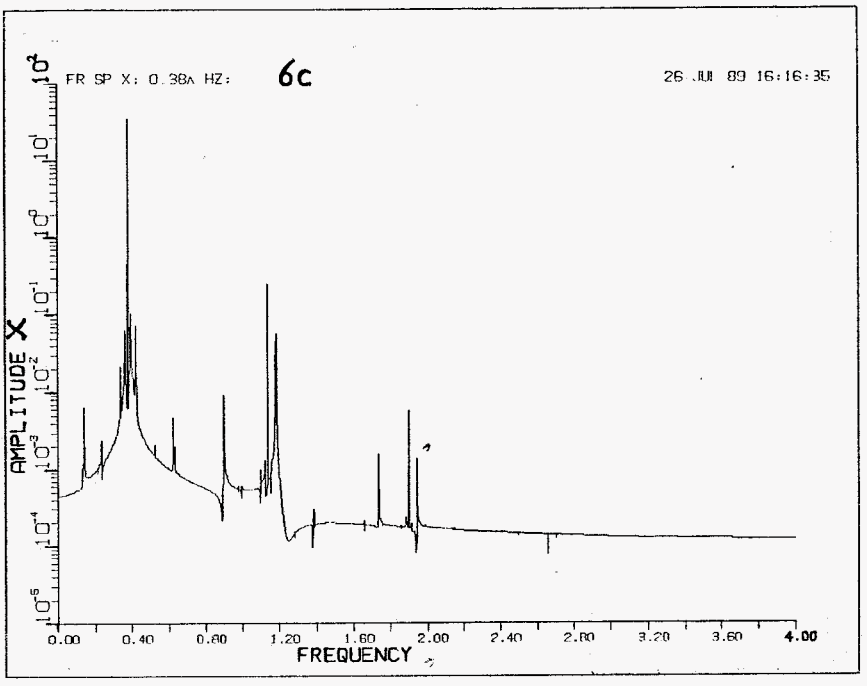

Fig. 3.12 *Frequency spectrum of x, high stable steady state, excitation* $F_x = \sin(2\pi\ 0.38\ t)$, *model 6C.*

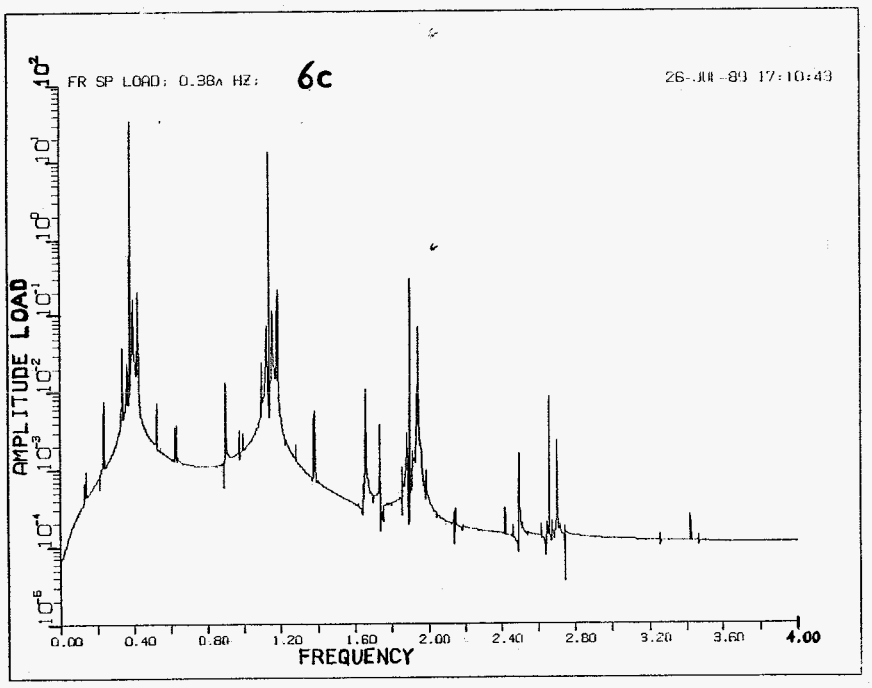

Fig. 3.13 *Frequency spectrum of* $F_x - F_{nl}$, *high stable steady state, excitation* $F_x = \sin(2\pi\ 0.38\ t)$, *model 6C.*

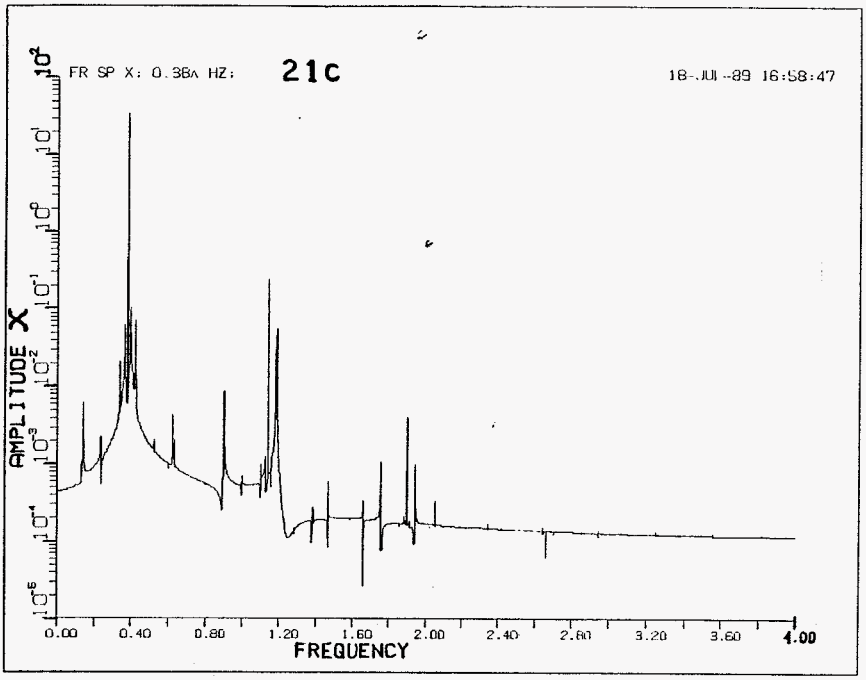

Fig. 3.14 *Frequency spectrum of x, high stable steady state, excitation* $F_x = \sin(2\pi\ 0.38\ t)$, *model 21C.*

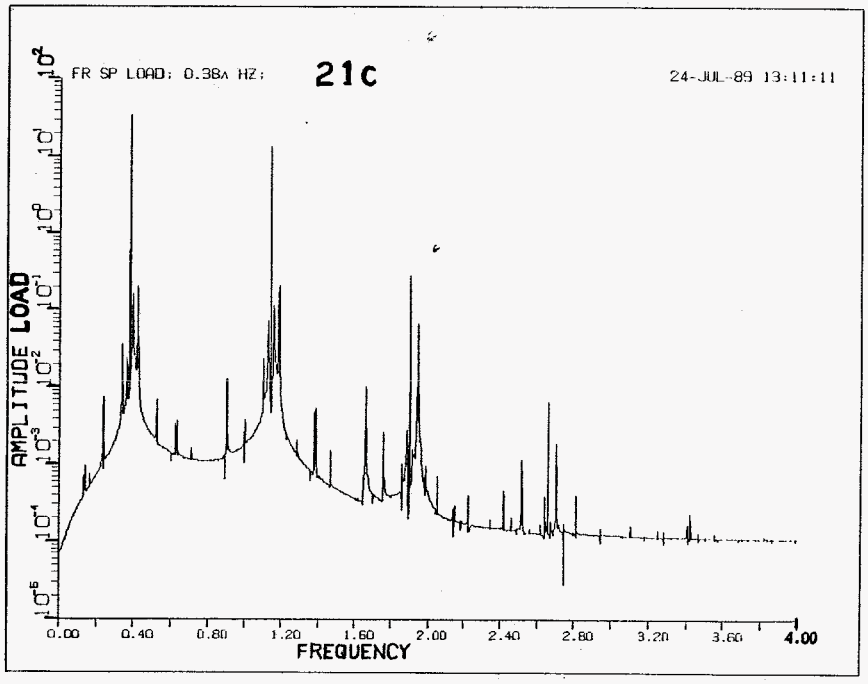

Fig. 3.15 *Frequency spectrum of* $F_x - F_{nl}$, *high stable steady state, excitation* $F_x = \sin(2\pi\ 0.38\ t)$, *model 21C.*

4. Periodic solutions of nonlinear dynamic systems combined with reduction of linear components.

The software program LIMSET (Crooijmans, 1987) has been developed for determining static, periodic (1 cyclic parameter) and quasi–periodic (2 cyclic parameters) equilibria of multidimensional nonlinear dynamic systems. Stable equilibria as well as unstable equilibria can be computed. The cyclic parameters may be free of forced. If the cyclic parameter is forced by a known periodic external load the frequency of this load is viewed as a design variable. In case the cyclic parameter is free, the corresponding frequency is unknown. In this paragraph we will restrict ourselfs to periodic equilibria with a forced cyclic parameter. Also methods, which are applied to judge stability and to detect bifurcation points, are not treated here.
The cyclic parameter τ is defined so, that the solution $\underset{\sim}{q}$ and the external load $\underset{\sim q}{f}$ are periodic with period 1:

$$\underset{\sim}{q}(\tau) = \underset{\sim}{q}(\tau + 1) \tag{4.1}$$

$$f_q(\tau) = f_q(\tau + 1) \tag{4.2}$$

τ is related to the real time t by:

$$\tau = tf = \omega t/2\pi \tag{4.3}$$

where f is the frequency of the periodic external load. Next to f other design variables may be defined, for example the cubic stiffness parameter of a nonlinear spring. The design variables, including f, are stored in column $\underset{\sim}{r}$. We will assume that all design variables, except for f, only are found in $\underset{\sim nl}{f}$ and $\underset{\sim q}{f}$. We rewrite the equations of motion (3.1) in terms of τ ($' = d/d\tau$):

$$f^2\, \underline{M}_q\, \underset{\sim}{q}''(\tau) + f\, \underline{B}_q\, \underset{\sim}{q}'(\tau) + \underline{K}_q\, \underset{\sim}{q}(\tau) + \tag{4.4}$$

$$\underset{\sim nl}{f}(\underset{\sim T}{x}'', \underset{\sim T}{x}', \underset{\sim T}{x}, \underset{\sim}{r}, \tau) = \underset{\sim q}{f}(\underset{\sim}{r}, \tau)$$

$$\text{or } \underset{\sim l}{F}\,(\underset{\sim}{q}''(\tau), \underset{\sim}{q}'(\tau), \underset{\sim}{q}(\tau), \underset{\sim}{r}, \tau) = \underset{\sim r}{F}\,(\underset{\sim}{r}, \tau)$$

Approximations for periodic solutions are calculated by application of a time

discretisation technique: velocities and accelerations are expressed in terms of displacements by means of difference schemes. Here we use an equidistant time grid with width of h and employ the central difference scheme with a consistency of $0(h^2)$:

$$\underset{\sim}{q}'(\tau_i) = (\underset{\sim}{q}(\tau_{i+1}) - \underset{\sim}{q}(\tau_{i-1}))/2h \tag{4.5}$$

$$\underset{\sim}{q}''(\tau_i) = (\underset{\sim}{q}(\tau_{i+1}) - 2\,\underset{\sim}{q}(\tau_i) + \underset{\sim}{q}(\tau_{i-1}))/h^2 \tag{4.6}$$

$$\tau_i = (i-1) * h \tag{4.7}$$

The width of the time grid h is determined by the number of discretisation points n_{dp}:

$$h = 1/n_{dp} \tag{4.8}$$

Periodicity is enforced by demanding that:

$$\underset{\sim}{q}(\tau_1) = \underset{\sim}{q}(\tau_{n_{dp}+1}) \tag{4.9}$$

In general it will be difficult to judge which factor is dominating the current accuracy: n_{dp} or the number of component modes. Substitution of the difference schemes in the n_q nonlinear differential equations (4.4) at discrete times τ_i (i=1, ..., n_{dp}) results in $n_{dp}*n_q$ nonlinear algebraic equations:

$$\underset{\sim}{G}(\underset{\sim}{z}, \underset{\sim}{r}) = \underset{\sim}{G}_l(\underset{\sim}{z}, \underset{\sim}{r}) - \underset{\sim}{G}_r(\underset{\sim}{r}) = \underset{\sim}{0} \tag{4.10}$$

$$\underset{\sim}{z} = [\underset{\sim}{q}(\tau_1)^T, \ldots, \underset{\sim}{q}(\tau_{n_{dp}})^T]^T \tag{4.11}$$

There are two possible ways to solve (4.10): by means of the Newton–Raphson algorithm or by application of the arc continuation method.

Newton–Raphson: If we assign a value to all design variables ($\underset{\sim}{r} = \underset{\sim}{r}_0$) we have as many equations as unknowns and an initial estimate, $\underset{\sim}{z}_0$, for the solution of (4.10) can be improved by the well–known iterative

Newton–Raphson process for multiple directions:

$$\underset{\sim}{G}_{,\underset{\sim}{z}}(\underset{\sim}{z}_i,\underset{\sim}{r}_0)\ \delta\underset{\sim}{z}_i = -\underset{\sim}{G}(\underset{\sim}{z}_i,\underset{\sim}{r}_0) \tag{4.12}$$

$$\underset{\sim}{z}_{i+1} = \underset{\sim}{z}_i + \delta\underset{\sim}{z}_i \tag{4.13}$$

The structure of the Jacobian $\underset{\sim}{G}_{,\underset{\sim}{z}}$ is shown in fig. 4.1. Much CPU time can be saved in solving (4.12) if use is made of the bandstructure of the upper left part of the Jacobian.

$\underset{\sim}{G}_{,\underset{\sim}{z}} =$

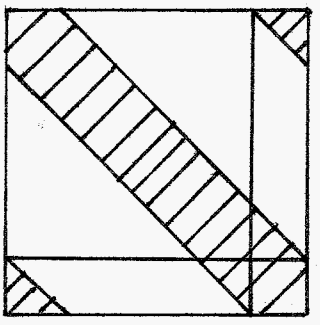

Fig. 4.1 Structure of the Jacobian.

The iterative process is stopped when some convergence criterion is satisfied. Of course, the calculated solution need not to be the only periodic solution of (4.10) for $\underset{\sim}{r} = \underset{\sim}{r}_0$. In general it will depend on the choice $\underset{\sim}{z}_0$. Furthermore the iteration process can fail because of three reasons:

1. Differential equations (4.4) have no periodic solution with period (lower than) 1. It is possible that there exist periodic solutions with a higher period (2,3,...). By demanding (4.9) however, subharmonic contributions to the solution are excluded and periodic solutions with periods higher than 1 cannot be found. Furthermore the solution can exhibit chaotic instead of periodic behaviour.
2. The Jacobian $\underset{\sim}{G}_{,\underset{\sim}{z}}$ is singular at the solution, which means that the solution is a bifurcation point.
3. $\underset{\sim}{z}_0$ is a bad estimate: the iterative process can diverge or the Jacobian can become singular at a local extremum. In this case more robust numerical procedures for solving nonlinear equations can be employed, see for example Marquardt (1963) and Powell (1970).

Arc continuation: By application of this method it is possible to investigate how a change in one design variable influences the periodic equilibrium. We choose for all design variables but the one we wish to change, say r, a value. Now (4.10) is reformulated by:

$$\underset{\sim}{G}\ (\underset{\sim}{z},\ r) = \underset{\sim}{0} \tag{4.14}$$

Starting from a periodic equilibrium $\underset{\sim}{z}_{e,1}$, $r_{e,1}$ determined with the Newton–Raphson algorithm, the direction in which the solution arc has to be followed is chosen depending on the wish to initially increase or decrease r.
Then a predictor step and several corrector steps are carried out to find a solution $\underset{\sim}{z}_{e,2}$, $r_{e,2}$ in the neighbourhood of $\underset{\sim}{z}_{e,1}$, $r_{e,1}$. This process is continued until r has reached a certain value.
In the predictor step the direction $\underset{\sim}{p}_z$, p_r of the line tangent to the solution arc at the point $\underset{\sim}{z}_{e,1}$, $r_{e,1}$ is determined by:

$$\underset{\sim}{G}_{,\underset{\sim}{z}}\ (\underset{\sim}{z}_{e,1},\ r_{e,1})\ \underset{\sim}{p}_z + \underset{\sim}{G}_{,r}\ (\underset{\sim}{z}_{e,1},\ r_{e,1})\ p_r = \underset{\sim}{0} \tag{4.15}$$

When the predictor step is carried out for the first time, p_r is set to 1 if r initially has to be increased. Otherwise p_r is set to –1. Now (4.15) can be solved for $\underset{\sim}{p}_z$ and the total solution $\underset{\sim}{p}_z$, p_r will be multiplied with a factor $\alpha>0$ so that the elliptical constraint:

$$\alpha^2\ (\underset{\sim}{p}_z^T\ \underset{\sim}{p}_z + p_r^2) = \sigma^2 \tag{4.16}$$

is satisfied, where σ is a well chosen step size. The prediction $\underset{\sim}{z}_p$, r_p can be calculated now:

$$\begin{bmatrix} \underset{\sim}{z}_p \\ r_p \end{bmatrix} = \begin{bmatrix} \underset{\sim}{z}_{e,1} \\ r_{e,1} \end{bmatrix} + \alpha \begin{bmatrix} \underset{\sim}{p}_z \\ p_r \end{bmatrix} \tag{4.17}$$

With following predictor steps σ may be altered using some stepsize criterion, see for example Allgower (1981). Furthermore the sign of α then will be chosen in such a way that the inner product of the present and preceding predictor directions is greater than zero, so that two successive predictor directions make a sharp angle and the solution arc is travelled in the same

direction all the time, provided that σ is not too large, see fig. 4.2.

In general the prediction $\underset{\sim}{z}_p$ (= $\underset{\sim}{z}_{c,0}$), r_p (= $r_{c,0}$) will not satisfy the convergence criterion. That's why the prediction is corrected:

$$\begin{bmatrix} \underset{\sim}{z}_{c,i+1} \\ r_{c,i+1} \end{bmatrix} = \begin{bmatrix} \underset{\sim}{z}_{c,i} \\ r_{c,i} \end{bmatrix} + \begin{bmatrix} \underset{\sim}{c}_{z,i} \\ c_{r,i} \end{bmatrix} \qquad (i = 0,1,...) \qquad (4.18)$$

The equations with which corrections $\underset{\sim}{c}_{z,i}$, $c_{r,i}$ are calculated look like the iterative Newton–Raphson equations:

$$\underset{\sim}{G}_{,\underset{\sim}{z}}(\underset{\sim}{z}_{c,i}, r_{c,i})\ \underset{\sim}{c}_{z,i} + \underset{\sim}{G}_{,r}(\underset{\sim}{z}_{c,i}, r_{c,i})\ c_{r,i} = \qquad (4.19)$$

$$- \underset{\sim}{G}(\underset{\sim}{z}_{c,i}, r_{c,i})$$

Because the number of unknowns is one more than the number of equations, an additional equation has to be formulated to make the set of equations solvable. We use the orthogonal trajectory method of Fried (1984) in which case the additional equation is given by:

$$c_{r,i} = (\underset{\sim}{G}_{,\underset{\sim}{z}}^{-1}(\underset{\sim}{z}_{c,i}, r_{c,i})\ \underset{\sim}{G}_{,r}(\underset{\sim}{z}_{c,i}, r_{c,i}))^T\ \underset{\sim}{c}_{z,i} \qquad (4.20)$$

This choice implies that the direction of the correction is orthogonal to the solution space of (see fig. 4.3):

$$\underset{\sim}{G}\ (\underset{\sim}{z}, r) - \underset{\sim}{G}\ (\underset{\sim}{z}_{c,i}, r_{c,i}) = \underset{\sim}{0} \qquad (4.21)$$

Corrections are carried out until the convergence criterion is fulfilled.

Until recently systems, which were analysed with LIMSET had a limited number of dof, because of high computing times and because of the fact that differential equations had to be supplied manually. By reducing linear components and coupling the ASKA program with LIMSET it seems possible to obtain approximations of periodic equilibria of complex dynamic systems with local nonlinearities. For illustration we will now investigate the steady state behaviour of the system presented in example 3.1.

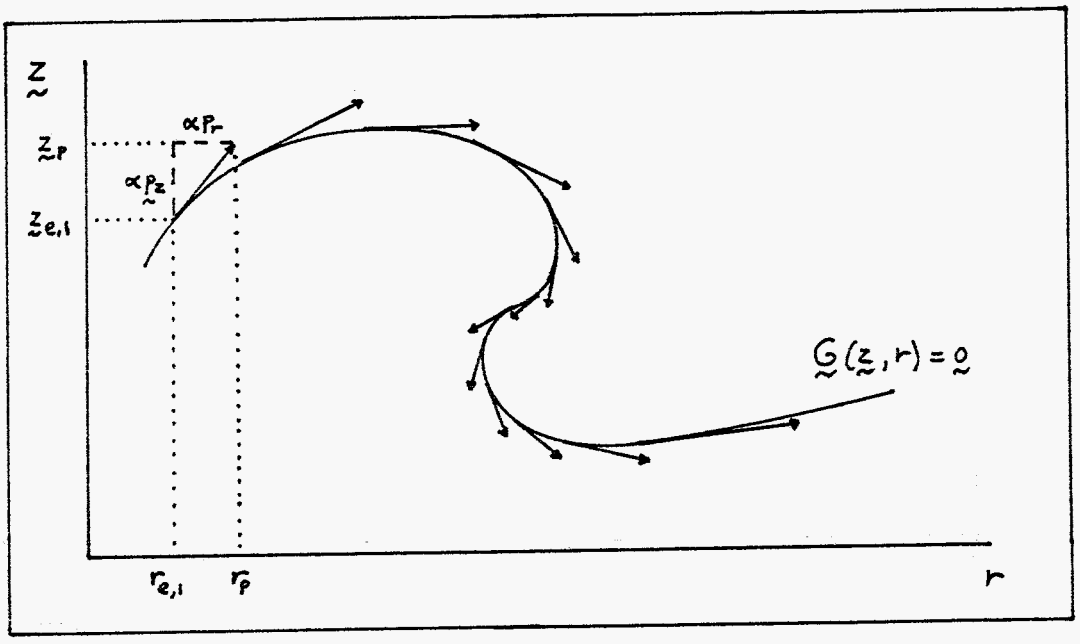

Fig. 4.2 Successive predictor directions make sharp angles.

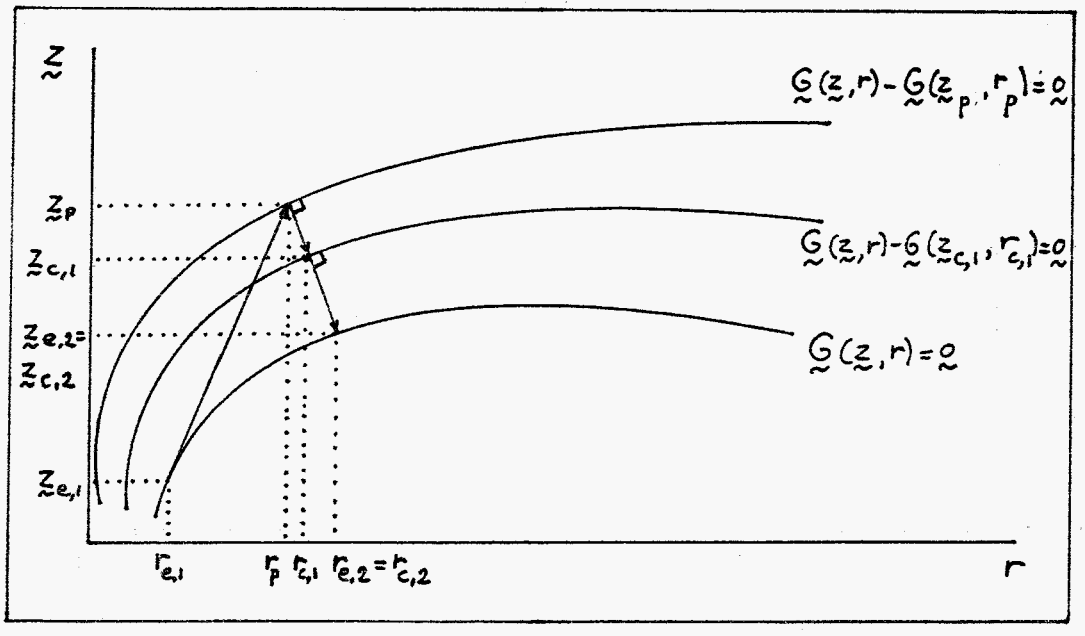

Fig. 4.3 Predictor–corrector mechanism in arc continuation method.

Example 4.1 (all quantities in SI units): The discrete mass of the system was loaded by the periodic external load $F_x = \cos(2\pi ft)$. By choosing f as the design variable to be varied we are able to calculate frequency response functions (frf). We studied the frf defined as the quotient of the absolute maximum displacement of the discrete mass and the amplitude of the external load (=1). The frf was calculated for two system models: (duffey)4A and (duffey)4C. With model 4A the bar was divided in 50 elements and reduced to 3 free interface eigenmodes plus 1 rf mode. Subsequently the internal load $F_{nl} = 0.5\ \ddot{x} + 0.02\ \dot{x} + 0.5\ x + 0.04\ x^3$ was added. Model 4C we already used in example 3.1. In table 4.1 the four lowest eigenfrequencies of the 50 dof system model are compared with those of the models 4A and 4C (all models without damper and nonlinear part of the spring!).

	50 dof	4A	4C
f_1	0.1504	0.1504	0.1504
f_2	0.3589	0.3589	0.3589
f_3	0.6187	0.6199	0.6187
f_4	0.8957	0.9648	1.0210

Table 4.1 Eigenfrequencies (Hz) of linear, undamped models.

The frf of 4A and 4C are shown in fig. 4.4 and fig. 4.5. In the calculations 40 discretisation points were used. Each analysis costed approximately 9000 s CPU time. In both figures the fourth peak was left out on purpose because with the linear undamped models 4A and 4C f_4 is an artificial eigenfrequency caused by the rf mode. The two figures look very similar with exception of the behaviour near 0.2 Hz, which will be explained later.
The first three small peaks can be identified as superharmonic resonances. They occur just above 1/3 f_1, 1/3 f_2 and 1/5 f_3. In fig. 4.6 of the three modal dof (p_i = coor. i) are shown together with the frf of x (= coor. 4) of model 4C. Clearly can be seen that p_1 is responsible for the peak near 1/3 f_1, p_2 for the peak near 1/3 f_2 and p_3 for the peak near 1/5 f_3. The relation between the dof is given by:

$$x = -0.883\ p_1 + 0.732\ p_2 + 0.482\ p_3 + 0.006\ p_B \qquad (4.22)$$

where p_B is the dof corresponding with the rf mode which was replaced by x

in (2.11). The fourth term on the right hand side of (4.22) appears to have little influence in the frequency range 0–0.2 Hz. Figures 4.7a–4.7f show the periodic solutions of x and the modal dof responsible for the superharmonic resonance mapped in phase space at 1/3 f_1, 1/3 f_2 and 1/5 f_3. We verified the superharmonic resonance at 1/3 f_2 by numerical integration of model 21C (see example 3.1). The result shown in fig. 4.8 covers completely fig. 4.7c. In table 4.2 the solutions calculated with LIMSET and numerical integration at 1/3 f_2 are compared.

	LIMSET (4C)	Num. Int. (21C)
frequency	0.1223	0.1211
max. displacement	2.805	2.727
max. velocity	3.962	3.919

Table 4.2. Comparison LIMSET – Numerical integration at 1/3 f_2.

Near 0.2 Hz we see in fig. 4.4 two peaks whereas in fig. 4.5 only one peak is found. This is caused by the fact that f_4 is lower with 4A than with 4C, which implies that the superharmonic solution at 1/5 f_4 occurs at a lower frequency with 4A. An annoying fact is that the superharmonic solution at 1/5 f_4 will not occur in reality because f_4 is an artificial eigenfrequency due to the rf mode. On the other hand the rf mode has positive influence near the anti–resonances. For example, consider the periodic solution of x at 0.2898 Hz, which has an amplitude of 0.0056 (4C). When x = + 0.0056, the sum of the first three terms on the right hand side of (4.22) is equal to – 0.0012, which remains for the last term 0.0068. Numerical integration of model 21C led to an amplitude of 0.0088 at this frequency.

Finally we look at the periodic solutions of x at 0.38 Hz (model 4C). At this frequency LIMSET found three periodic solutions of which two are stable (amplitudes 1.049 and 6.248) and one is unstable (amplitude 5.176). The two stable periodic solutions we already calculated by means of numerical integration in example 3.1. With model 21C we found during the last 300 s. of the two numerical integration calculations as maximum displacements: 1.038 respectively 6.241.

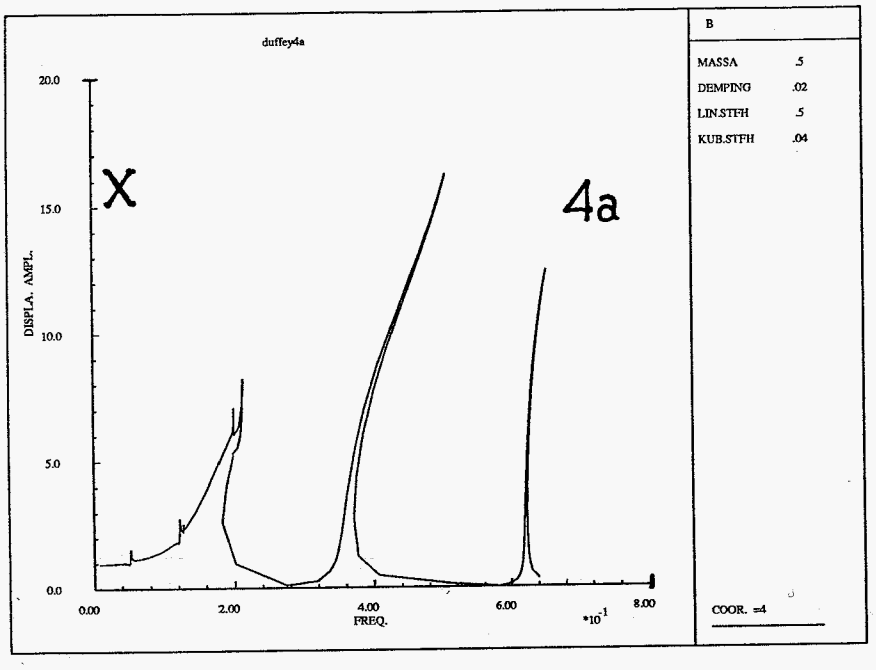

Fig. 4.4 Frequency response function, model 4A.

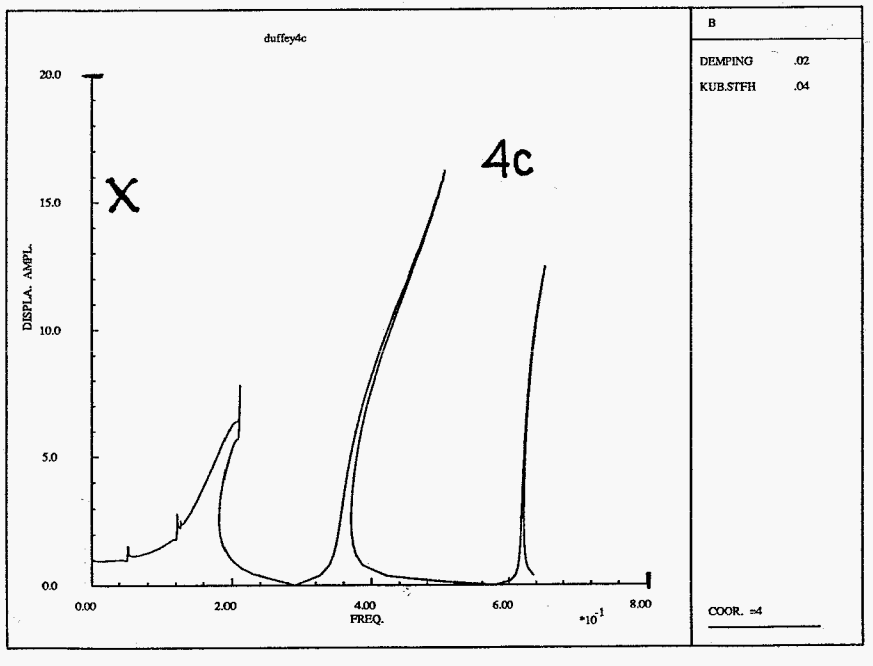

Fig. 4.5 Frequency response function, model 4C.

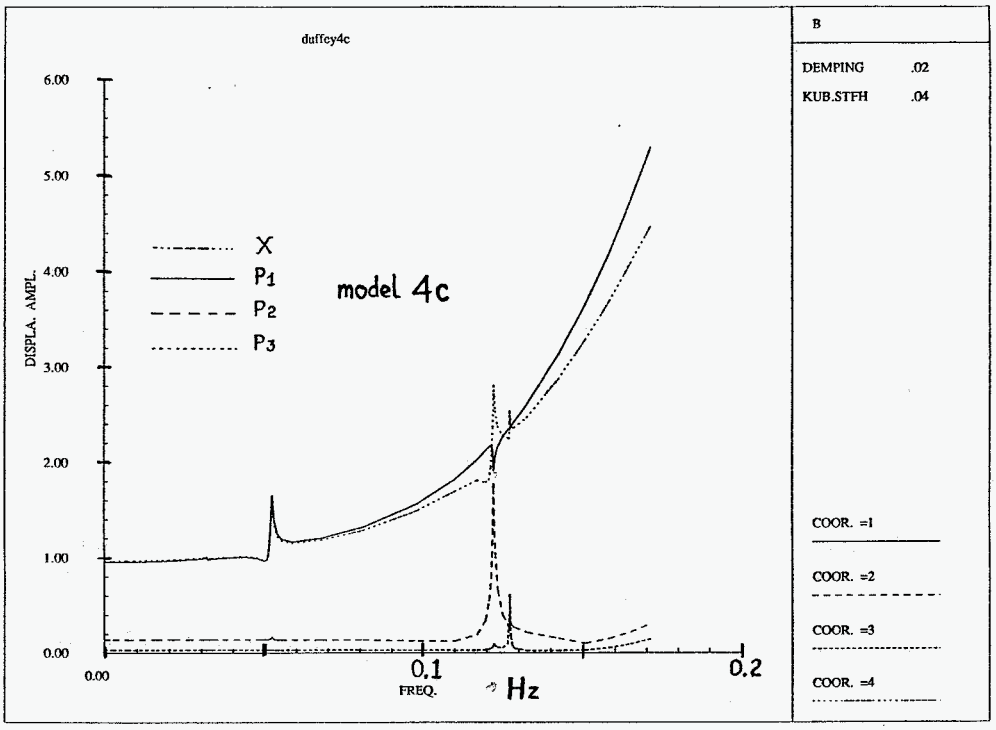

Fig. 4.6 Superharmonic resonances near 1/3 f_1, 1/3 f_2 and 1/5 f_3; Contributions of modal dof p_1, p_2 and p_3 to the frf of x.

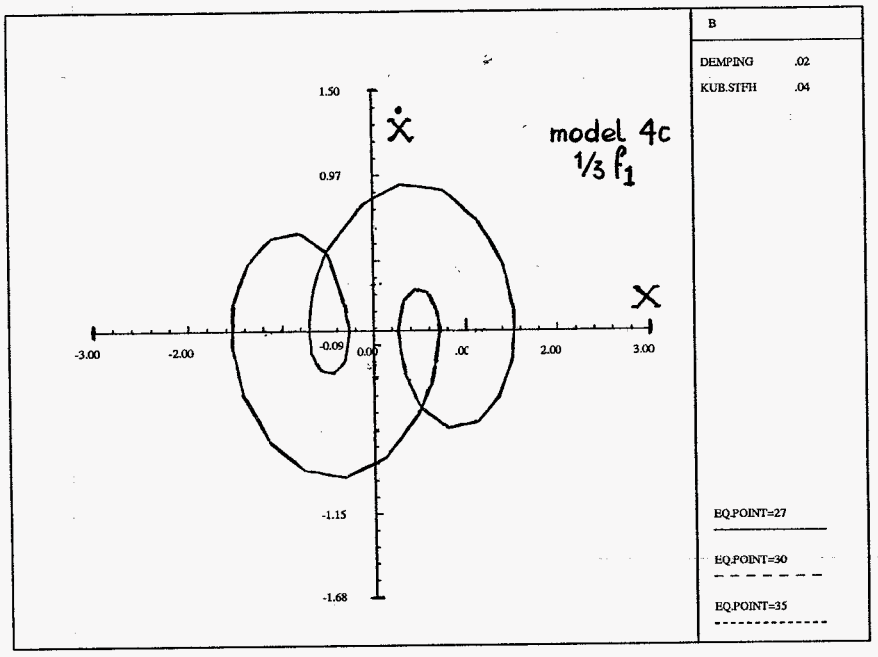

Fig. 4.7a Phase portrait of periodic solution of x near 1/3 f_1.

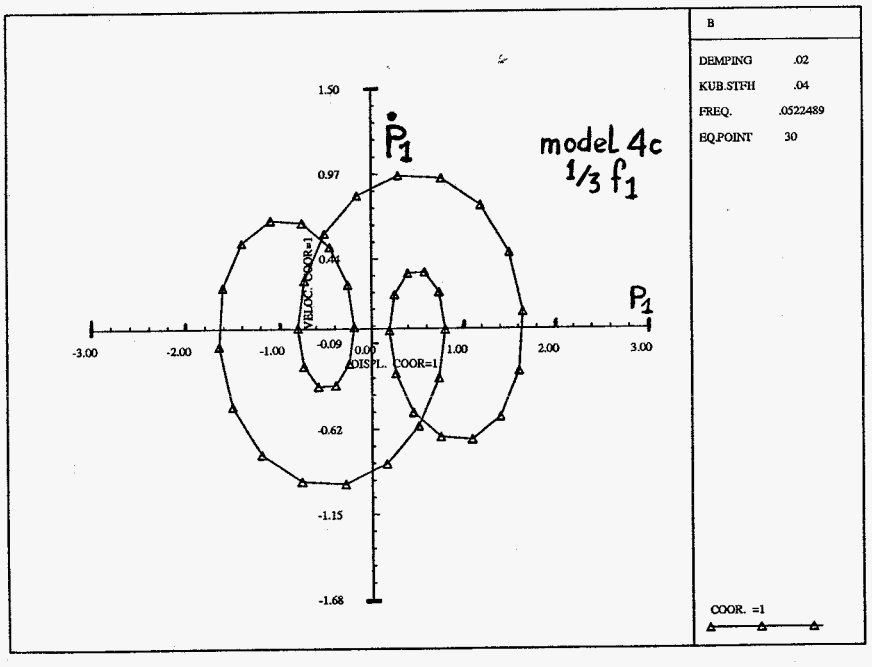

Fig. 4.7b Phase portrait of periodic solution of p_1 near 1/3 f_1.

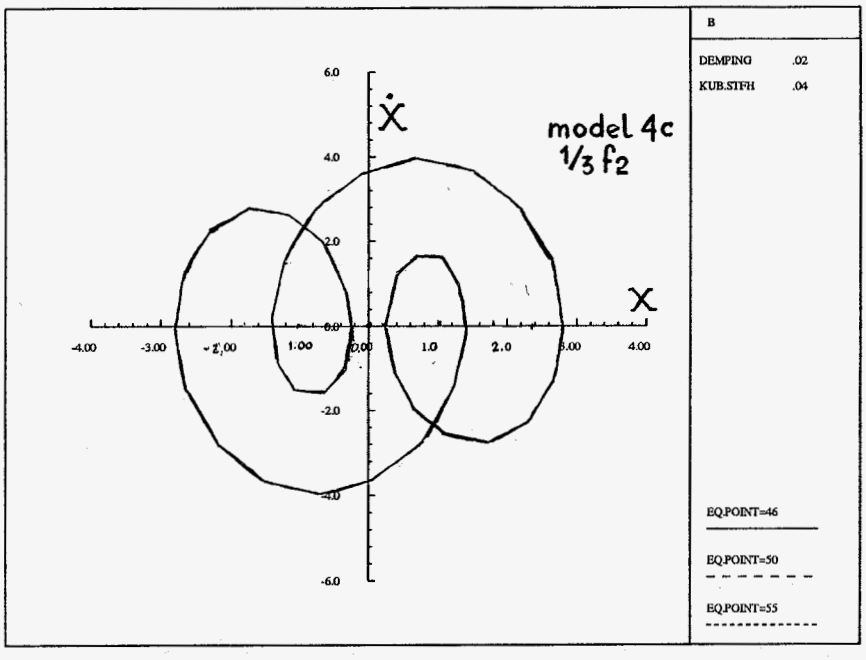

Fig. 4.7c Phase portrait of periodic solution of x near 1/3 f_2.

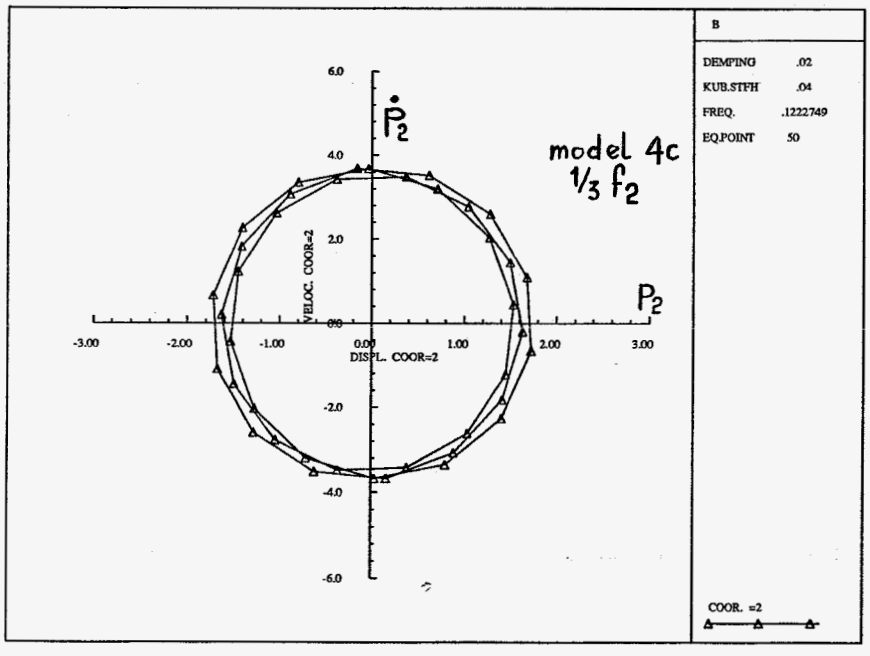

Fig. 4.7d Phase portrait of periodic solution of p_2 near 1/3 f_2.

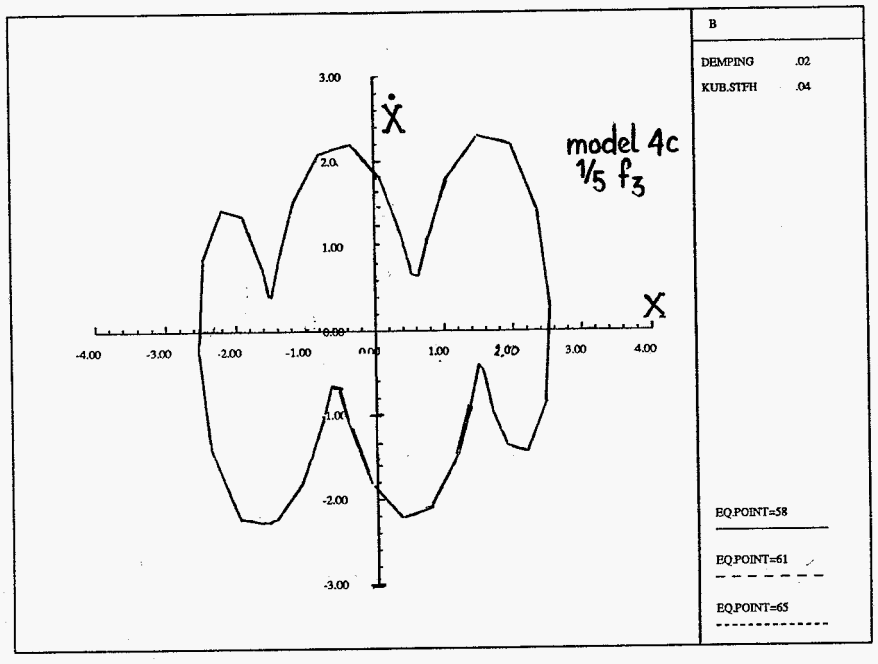

Fig. 4.7e Phase portrait of periodic solution of x near 1/5 f_3.

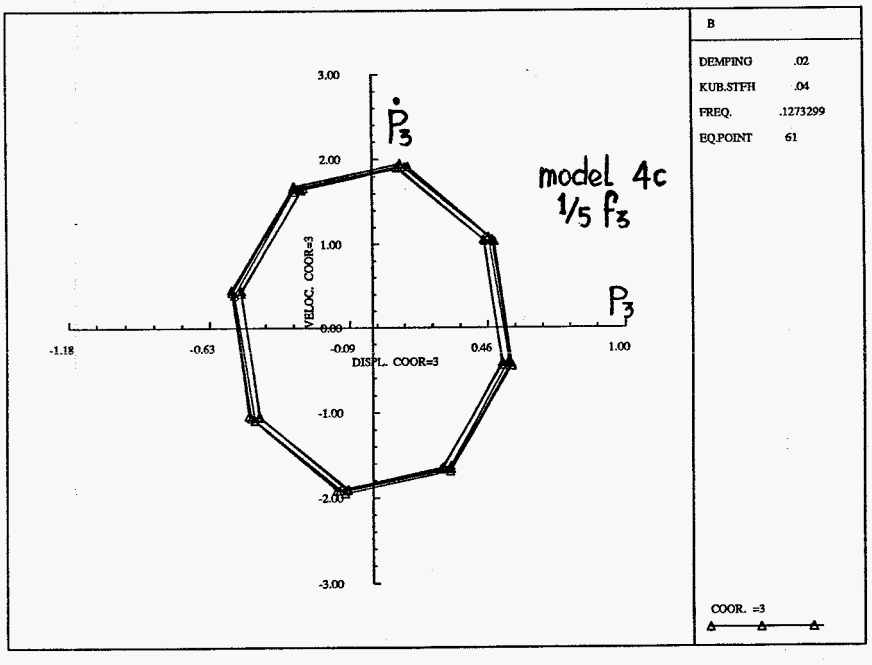

Fig. 4.7f Phase portrait of periodic solution of p_3 near 1/5 f_3.

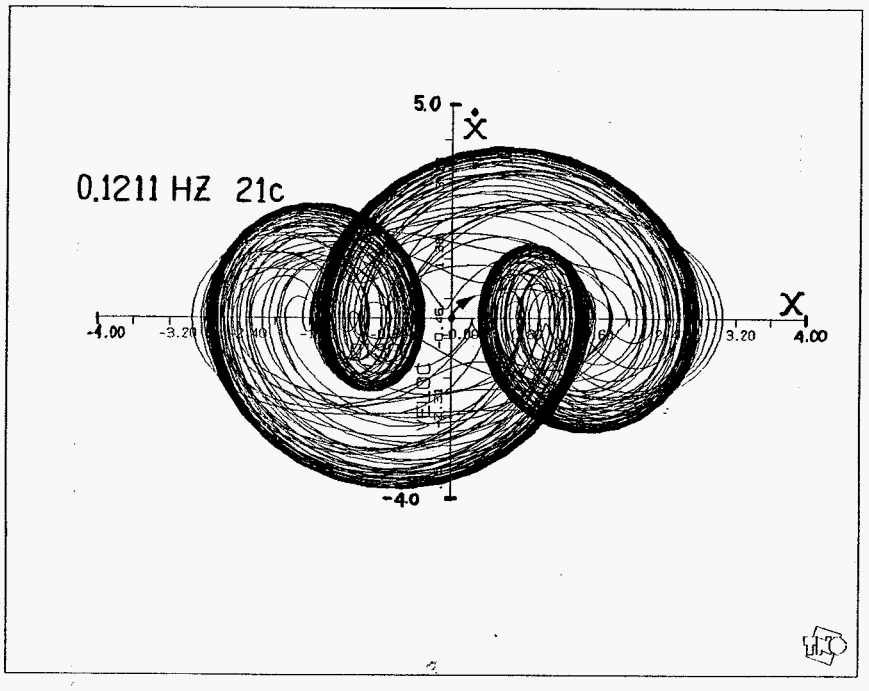

Fig. 4.8 *Phase portrait of periodic solution of x near 1/3 f_2 calculated by numerical integration, model 21C.*

5. Review and conclusions.

We end this report by reviewing what has been treated and drawing some conclusions:

1) A cms method which makes use of free interface eigenmodes and residual flexibility modes is presented. With this method a frequency criterion can be applied at component level to reduce systems consisting of linear components. Using this method a lot of CPU time can be saved in an eigenvalue analysis if identical components are present.
2) A strategy has been proposed for sensible reduction of systems, consisting of linear components and local nonlinearities. It has been applied succesfully to a system with a local nonlinearity of the Duffing type. The amount of CPU time that could be saved in a time integration analysis by reducing the linear component was considerable.
3) A finite difference method for determination of periodic solutions of nonlinear dynamic systems is combined with the reduction technique for linear components. In the example of the system with the local nonlinearity of the Duffing type solutions calculated with this method corresponded well with numerical integration solutions.
4) With systems of the Duffing type artificial eigenfrequencies above the cut–off frequency f_c cause superharmonic resonances below f_c which will not occur in reality. Therefore it should be considered to truncate the system eigenfrequencies above f_c after coupling of reduced linear components. A consequence of this is that the response near anti–resonances will become less accurate.

References:

* Allgower, E.L.; A survey of homotopy methods for smooth mappings, From: 'Numerical solutions of nonlinear equations', Proceedings Bremen, 1980, Eds. Allgower, Glashoff, Petigen, Lecture notes in mathematics nr. 878, Springer–Verlag, 1981, pp. 1–29.

* ASKA Saab–Scania/Ikoss User's Manual, 1986.

* Craig, R.R.Jr.; A review of time–domain and frequency–domain component mode synthesis method. From: 'Combined experimental/analytical modeling of dynamic structural systems (AMD–Vol. 67)' edited by Martinez and Miller, 1985, pp. 1–30.

* Crooijmans, M.T.M.; On the computation of stationary deterministic behaviour of non–linear dynamic systems with applications to rotor–bearing structures, Thesis, Eindhoven Univesity of Technology, The Netherlands, 1987.

* Fey, R.H.B.; Dynamische reductie en koppeling van substructuren, WFW–rapport 87.028, Eindhoven University of Technology, The Netherlands, 1987 (in Dutch).

* Fried, I.; Orthogonal trajectory accession to the nonlinear equilibrium curve, Computer methods in applied mechanics and engineering 47, 1984, pp. 283–297.

* Langeveld, C.J.; Een koppelingsmethode voor mechanische componenten, TNO–rapport 5025002–86–1, TNO–IWECO, Delft, The Netherlands, 1986 (in Dutch).

* Marquardt, D.W.; An algorithm for least–squares estimation of nonlinear parameters, J. Soc. Indust. Appl. Math. Vol.11 No.2, 1963.

* Morris, A.; Selected results from the NAFEMS dynamics working group free vibrations Benchmarks – part 1, Benchmark NAFEMS, april 1989, pp. 12–19.

* NAG FORTRAN Library Manual, Mark 13, 1988.

* Powell, M.J.D.; A hybrid method for nonlinear equations, In: 'Numerical methods for nonlinear algebraic equations', Rabinowitz, P. (ed), Gordon and Beach, 1970.